ACS APPLIED MATERIALS & INTERFACES

Research Article

www.acsami.org

Enhancing Stability of Perovskite Solar Cells to Moisture by the Facile Hydrophobic Passivation

Insung Hwang,[†] Inyoung Jeong,[§,‡] Jinwoo Lee,[§] Min Jae Ko,[‡,⊥] and Kijung Yong*[,†]

[†]Surface Chemistry Laboratory of Electronic Materials, Department of Chemical Engineering, Pohang University of Science and Technology (POSTECH), Hyoja-Dong, Pohang-Si 790-784, Republic of Korea

[§]Advanced Functional Nanomaterial Laboratory, Department of Chemical Engineering, Pohang University of Science and Technology (POSTECH), Hyoja-Dong, Pohang-Si 790-784, Republic of Korea

[‡]Photo-Electronic Hybrids Research Center, Korea Institute of Science and Technology (KIST), Seoul 136-791, Republic of Korea

[⊥]KU-KIST Graduate School of Converging Science and Technology, Korea University, Seoul 136-701, Republic of Korea

Supporting Information

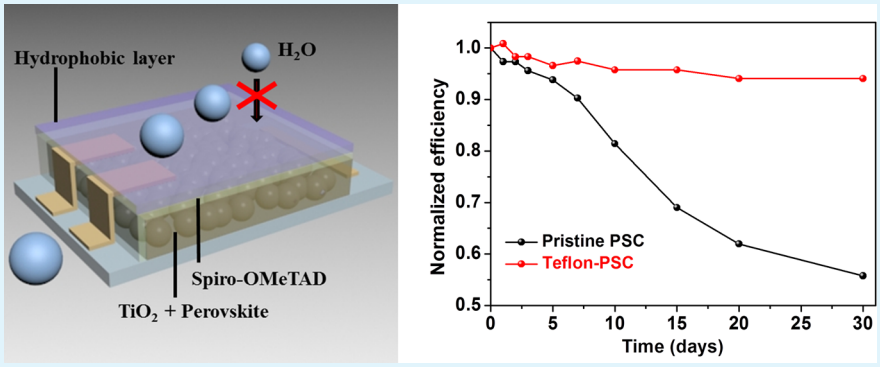

ABSTRACT: In this study, a novel and facile passivation process for a perovskite solar cell is reported. Poor stability in ambient atmosphere, which is the most critical demerit of a perovskite solar cell, is overcome by a simple passivation process using a hydrophobic polymer layer. Teflon, the hydrophobic polymer, is deposited on the top of a perovskite solar cell by a spin-coating method. With the hydrophobic passivation, the perovskite solar cell shows negligible degradation after a 30 day storage in ambient atmosphere. Suppressed degradation of the perovskite film is proved in various ways: X-ray diffraction, light absorption spectrum, and quartz crystal microbalance. This simple but effective passivation process suggests new kind of approach to enhance stability of perovskite solar cells to moisture.

KEYWORDS: *perovskite solar cell, stability, hydrophobicity, passivation, encapsulation, degradation of perovskite*

INTRODUCTION

Recently, $CH_3NH_3PbI_3$ perovskite has been one of the most promising materials for the absorber layer in solar cells. $CH_3NH_3PbI_3$ perovskite has diverse advantages, such as a high absorption coefficient,[1] a strong dipole moment causing rapid electron transport,[2] an ideal band gap energy of ∼1.5 eV,[3] simple and various synthetic methods,[4,5] the ability to transport the hole and the electron,[6] and low cost of synthesis from solution processes. On the basis of these advantages, significant attention has been focused on $CH_3NH_3PbI_3$ over the past few years.[7−9]

The first photovoltaic application of perovskite was reported by Kojima et al. in the form of a dye-sensitized solar cell with the liquid electrolyte and dye replaced by the perovskite.[10] The first reported power conversion efficiency (PCE) of the perovskite solar cell (PSC) based on $CH_3NH_3PbI_3$ was 3.8%. N.G. Park et al. have reported an increased efficiency of 6.5% with the liquid type of the electrolyte,[1] followed by a first report of the solid-state perovskite cell with an increased PCE of 9.7% and the improved stability by substitution of the solid hole transporting material (HTM) for liquid electrolyte.[11] Subsequently, an enormous surge in research on the perovskite solar cell occurred. Through various studies, the best reported PCE of the perovskite solar cell has reached 20%.[12] In only a few years, an incredible increase in the PCE of the perovskite solar cell has been achieved.

Unfortunately, $CH_3NH_3PbI_3$ perovskite has an intrinsic problem regarding long-term stability, especially when it is exposed to light or water (humidity). An intercalated polar molecule in the perovskite, $CH_3NH_3^+$, has a tendency to easily diffuse from the perovskite in the presence of a polar solvent. Additionally, the mechanism of perovskite decomposition

Received: May 24, 2015
Accepted: July 8, 2015
Published: July 8, 2015

DOI: 10.1021/acsami.5b04490
ACS Appl. Mater. Interfaces 2015, 7, 17330−17336

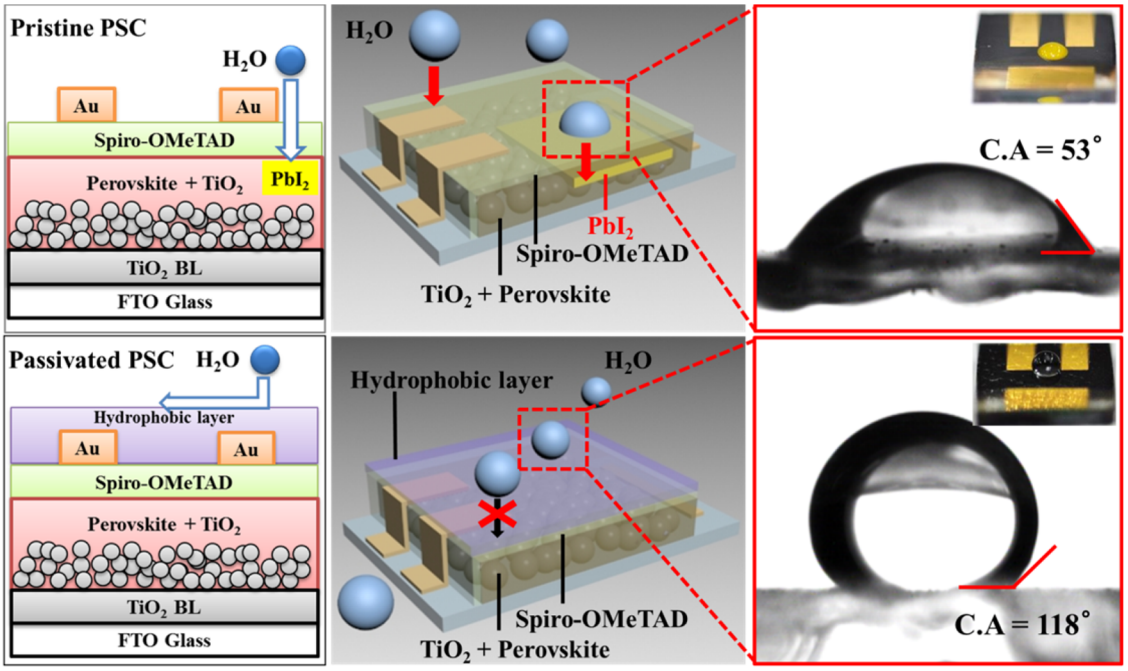

Figure 1. From left, schematic illustration showing the principle of hydrophobic passivation, contact angles of the untreated cell (top) and passivated cell (bottom), digital photographs of both cells showing contact angles. Also insets show water drop on cell surfaces. Yellow color of water drop on untreated cell is caused by dissolution of perovskite by water.

under light illumination has been suggested.[13] As M. Grätzel has commented,[14] relatively limited research has been conducted on the stability enhancement, although it is significantly required.

There has been some research from efforts to fabricate more stable PSCs.[15] For example, Seok and co-workers modified the crystal structure of $CH_3NH_3PbI_3$ perovskite by introducing Br, to synthesize $CH_3NH_3Pb(I_{1-x}Br_x)_3$, which is known to be more stable than $CH_3NH_3PbI_3$.[16] Also, Karunadasa et al. have developed new type of stable hybrid perovskite, $(PEA)_2(MA)_2Pb_3I_{10}$ (PEA is $C_6H_5(CH_2)_2NH_3^+$ and MA is $CH_3NH_3^+$).[17] Habisreutinger et al. applied carbon nanotube/polymer composites into HTM to produce thermally stable PSC.[18] Xiao et al. introduced polyaniline HTM to PSCs and exhibited considerable long-term stability of the cell.[19] Though there have been reported some other studies on stability of PSCs,[20,21] still it is necessary to improve the stability of PSCs. Moreover, even though PSCs is considerably vulnerable to the moisture, there have been reported few studies adopting the concept of hydrophobicity.[18]

In this study, we report a simple and effective passivation method for the perovskite solar cell. To overcome water vulnerability of perovskite we have introduced a concept of hydrophobicity to the passivation process. This passivation method, or might be considered as polymer encapsulation, has previously proved its potential in the work of Javey et al. on transistors.[22] By coating a hydrophobic film onto the top surface of the cell, water diffusion into the perovskite cell was effectively blocked. Water infiltration was simultaneously prevented chemically (repulsion on the molecular level by the hydrophobicity) and physically (encapsulation on the macroscopic level). Through hydrophobic passivation, the perovskite solar cell showed a significantly enhanced stability under ambient atmosphere conditions. The cell also showed stable behavior over a certain time while it was even immersed in water. The passivation was completed through a simple process, suggesting a promising probability of practical application. This facile passivation process would make a synergy with a further encapsulation process, providing PSC much improved stability.

EXPERIMENTAL SECTION

A conventional PSC was fabricated using the typical two-step method, as previously reported.[4] A compact layer of TiO_2 and a mesoporous layer of TiO_2 were deposited on patterned FTO glass through spin-coating and calcination. On the mesoporous TiO_2 layer with a thickness of ~300 nm, PbI_2 film was deposited by spin-coating of a 1 M *N*,*N*-dimethylformamide solution of PbI_2 for 30 s. Then, the film was immersed in a methylammonium iodide solution in isopropyl alcohol solvent with a concentration of 10 mg/mL for 30 s, resulting in the self-assembly of the perovskite film on the TiO_2 layer. Spiro-OMeTAD was adopted as the HTM layer and was deposited onto the perovskite layer by spin-coating of the prepared solution with the previously reported composition.[23] Au was thermally evaporated onto the Spiro-OMeTAD layer to be used as the top contact. Teflon AF (Teflon) was deposited onto the top of the entire cell by spin-coating of the Teflon precursor solution. Commercial Teflon precursor solution was purchased from DuPont (DuPont AF, amorphous fluoroplastics solution, GRADE 400S2-100-1) and used without further treatment. A small area of Au top contact was masked before the Teflon coating to provide an electrical contact. A Teflon layer was deposited during the spin-coating with the spin rate of 500 rpm for 20 s. After the spin-coating of Teflon, the cell was dried in a 70 °C oven for 30 min. The fabricated cells from the above processes were used in *J*–*V* measurements. For the XRD and QCM measurements, the samples were prepared in the same manner as mentioned above. For XRD, the FTO/compact TiO_2/mesoporous TiO_2/perovskite/Spiro-OMeTAD sample and the FTO/compact TiO_2/mesoporous TiO_2/perovskite/Spiro-OMeTAD/Teflon sample were prepared using a method identical to that explained above, except the thermal evaporation of the Au top contact inevitably omitted. The entire process was identically applied to the fabrication of samples for the QCM measurement.

The contact angle measurement was conducted with the Kruss, Model DSA-10 system. Light absorption spectrum was provided by the measuring equipment (Mecasys Co., OptizenPOP). X-ray

DOI: 10.1021/acsami.5b04490
ACS Appl. Mater. Interfaces 2015, 7, 17330−17336

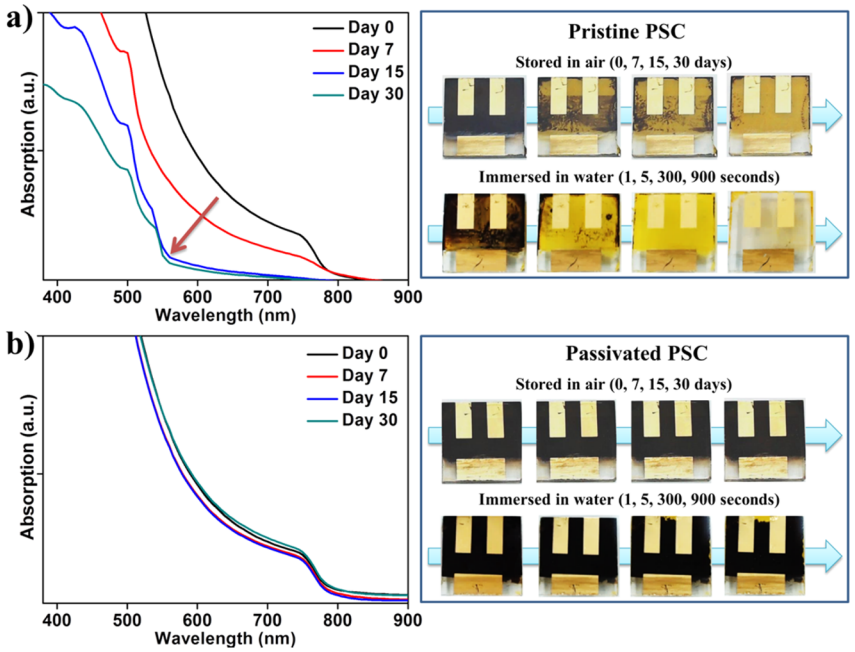

Figure 2. (a) Light absorption spectrum of the pristine perovskite film, as-prepared and after storage in air ambient for 7, 15, and 30 days. Digital photographs of PSC observed at regular time intervals in air and submerged underwater conditions. (b) Light absorption spectrum of the Teflon-passivated perovskite film, as-prepared and after storage in air ambient for 7, 15, and 30 days. Digital photographs of the passivated PSC observed at regular time intervals in air and submerged underwater conditions.

diffraction patterns were obtained by the XRD equipment (D/MAX-2500/PC). Mass change was observed with QCM equipment (QCM200, Stanford Research Systems Inc.). The $I-V$ measurement was performed through a solar simulator (ABET Tech., Sun 3000) and a potentiostat (IVIUM Tech.). The active area of PSCs was 0.12 cm^2 and the illumination condition was AM 1.5G (100 mW cm^{-2}). All the $I-V$ measurements of main text was conducted under the same condition of scan direction of backward scan: scan range of from −1.1 to +0.2 V, and scan rate of 0.1 V/s, ignoring the hysterisis behavior of conventional PSCs. The hysterisis behaviors of the initial PSCs were investigated and covered in the Supporting Information, according to the previous literature where hysteresis behavior of PSCs are profoundly investigated.[24]

RESULTS AND DISCUSSIONS

Conventionally, the hydrophilicity and hydrophobicity of a surface is determined by the contact angle (CA) of a single droplet of water on the surface. The contact angle is the angle at which a liquid interface meets a solid surface. According to the convention in the field of surface chemistry, a surface is defined as superhydrophilic when the CA is lower than ∼10°, whereas it is hydrophilic when the CA is between 10° and 90°. However, the surface is classified as hydrophobic when the CA is over the range of 90° to ∼150°. When the surface shows extremely hydrophobic behavior with the CA over 150°, it is defined as a superhydrophobic surface.

Figure 1 shows the hydrophobic characteristics of the Teflon-coated perovskite solar cell through the contact angle measurements. The contact angles of the water droplets on the surfaces of the perovskite solar cells were measured with and without the hydrophobic passivation. For the solar cell without the hydrophobic passivation, a small droplet of water (∼10 μL) formed a relatively hydrophilic contact with the cell, proven by the estimated CA of 53°. Moreover, a few minutes later, diffusion of the droplet into the hole-transporting material (HTM) and the perovskite film was observed, which results in degradation of the perovskite film. The yellow droplet in the digital photograph in the Figure 1 inset supports this observation. However, a considerably hydrophobic behavior was observed in the cell with the Teflon-treatment, showing a CA of 118°. Through the passivation with Teflon, diffusion of water and humidity from the top side of the perovskite solar cell could be effectively blocked. The stability of the cell was accordingly enhanced, which was proven by the following analyses.

As previously reported,[5] methylammonium lead halide perovskite film is formed through intercalation of methylammonium ions into the lattice space of PbI_2. Although the intercalation is a favorable reaction, if the film is exposed to water or other polar solvents, dissolution of the polar organic $CH_3NH_3^+$ in the perovskite structure could occur. This process is the main cause of degradation of perovskite in a humid atmosphere. According to the previous studies,[25] the whole degradation process can be expressed as following equations:

$$CH_3NH_3PbI_3(s) \leftrightarrow PbI_2(s) + CH_3NH_3I(aq) \quad (1)$$

$$CH_3NH_3I(aq) \leftrightarrow CH_3NH_2(aq) + HI(aq) \quad (2)$$

$$4HI(aq) + O_2(g) \leftrightarrow 2I_2(s) + 2H_2O(l) \quad (3)$$

$$2HI(aq) \leftrightarrow H_2(g) + I_2(s) \quad (4)$$

which leaves PbI_2 semiconductors with a band gap energy of ∼2.3 eV. Because the $CH_3NH_3PbI_3$ perovskite has a band gap energy of ∼1.5 eV and a corresponding dark brown color, the degradation degree of perovskite can be easily and generally estimated by observing the change of the crystal color from dark brown to yellow (the color of PbI_2).

Time-dependent changes of the optical properties of the untreated perovskite solar cell (PSC) and Teflon-treated PSC were observed by light absorption spectrum measurement and a digital camera-based visual observation, as shown in Figure 2.

DOI: 10.1021/acsami.5b04490
ACS Appl. Mater. Interfaces 2015, 7, 17330−17336

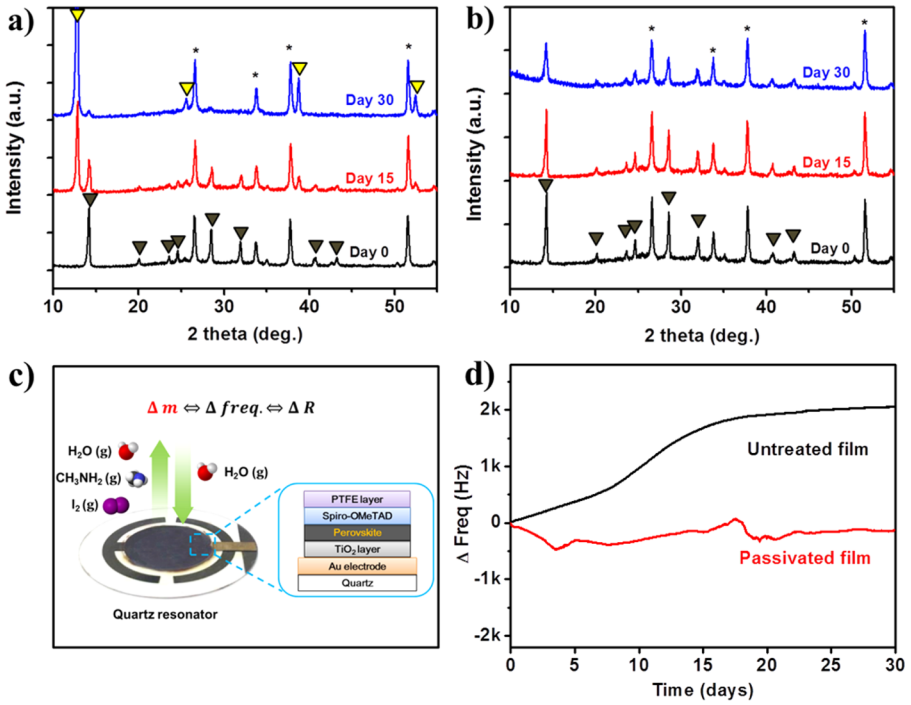

Figure 3. (a) Time-dependent XRD patterns of the FTO/TiO_2/$CH_3NH_3PbI_3$/Spiro-OMeTAD films stored in air. (b) Time-dependent XRD patterns of the FTO/TiO_2/$CH_3NH_3PbI_3$/Spiro-OMeTAD/Teflon films in air. (*, peaks from FTO; yellow mark, peaks from PbI_2; dark brown marks, peaks from perovskite). (c) Schematic illustration showing the prepared sample for the QCM measurement. Two samples were prepared with and without the Teflon layer on the top. Changes of the mass of the film on the QCM resonator resulted in changes of the frequencies and were detected by the externally connected electric sensor. (d) Obtained frequency change curves for the pristine perovskite film and Teflon-passivated perovskite film (initial frequency was 4950 kHz).

For the light absorption spectroscopy, both films of FTO/TiO_2/perovskite/HTM and FTO/TiO_2/perovskite/HTM/Teflon were prepared and their light absorption spectra were measured right after the film preparations and after 7, 15, and 30 days of storage in an ambient atmosphere. The light absorption spectrum of the film without the passivation is shown in Figure 2a, showing considerable time-dependent blue-shift of the absorption peak. The as-prepared film (day 0) exhibited absorption onset at the wavelength of ~780 nm. This onset wavelength can be translated to the band gap energy of ~1.59 eV (according to the well-known relationship between band gap energy and wavelength: $E_G = 1240/\lambda_{onset}$), which coincides well with previously reported band gap energy of $CH_3NH_3PbI_3$ perovskite.[26] However, as the storage time increased the absorption onset by perovskite diminished and the onset by PbI_2 at ~540 nm became distinct instead. The corresponding optical color change of PSC is shown in the right side of the spectrum. Over time, severe and rapid degradation of the untreated PSC was observed as shown in drastic color changes, and finally, the entire conversion of perovskite into PbI_2 was observed after approximately 30 days when it was stored under typical indoor conditions.

In contrast, as shown in Figure 2b the hydrophobically passivated film exhibited no change in the light absorption spectrum, showing a significantly enhanced stability to the humidity. This enhanced stability was confirmed again by the visual observation, as shown in the right side of Figure 2b. During storage for 30 days in an ambient atmosphere, no change of color was found for the hydrophobically passivated PSC. Moreover, the passivated cell exhibited a water-repellent property, even in submerged underwater conditions. The untreated cell showed immediate color changes due to dissolution-caused cell degradation right after immersion in water, whereas the passivated cell showed no color changes with a strong stability under water, blocking the penetration of the water for more than 900 s. Note that a very slight sign of degradation of perovskite was observed at the edges of the device. This was caused by the water infiltration through the inevitably exposed area of the device: side area. Although the polymer layer effectively blocked the water infiltration through the normal direction of the cell, a very little amount of water had infiltrated through the edges of the cell. If the edges of the device are sealed by other simple fabricating step, this result suggests a promising solution for overcoming water vulnerability of the perovskite cell by a simple hydrophobic passivation.

In addition to the general estimation by the optical observation above, more decisive information on the degradation of both of the cells was obtained from the X-ray diffraction (XRD) peak analysis and the quartz crystal microbalance (QCM), as provided in Figure 3. For the XRD measurement, the TiO_2 layer was deposited on a FTO glass followed by the deposition of a perovskite layer and Spiro-OMeTAD. Structures of the samples for XRD analysis were identical to a real perovskite solar cell, except for the absence of the top Au contact. Two samples were prepared as described above, and one of the samples underwent the hydrophobic passivation treatment. Because of the amorphous structures of Spiro-OMeTAD and the passivation layer, it was possible to measure the XRD spectrum for the inner perovskite layer without any interference of the outer layers

Figure 3a,b shows the obtained XRD patterns from the untreated and passivated perovskite films. Certain insignificant peaks were found from FTO, which are located at 26.5°, 33.7°,

DOI: 10.1021/acsami.5b04490
ACS Appl. Mater. Interfaces 2015, 7, 17330−17336

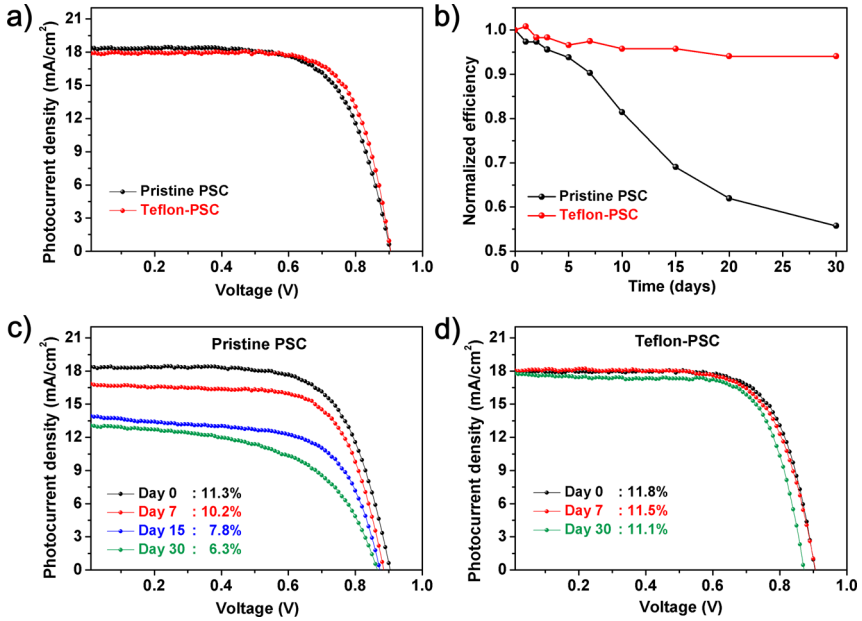

Figure 4. (a) $J-V$ curves of untreated PSC and Teflon-PSC. (b) Normalized PCE changes of both of the PSCs. (c) Changes of $J-V$ curves of the untreated PSC for 30 days. (d) Changes of $J-V$ curves of hydrophobically passivated PSC for 30 days.

37.9°, and 51.6° (the (110), (101), (200), and (211) planes of FTO, respectively, proven by the reference of JCPDS #77-0447). In the graphs, these peaks are indicated by asterisks and should be removed from consideration. For the untreated film, many obvious characteristic peaks of the perovskite film were observed on the day of sample preparation. Peaks of the perovskite film were found at 14.2°, 20.2°, 23.6°, 24.7°, 28.5°, 32°, 40.8°, and 43.3°, which exactly coincide with previously reported XRD peak patterns in other studies.[27,28] However, after a 15 day storage, the XRD patterns exhibited a different aspect, as clearly seen in Figure 3a. As marked with yellow indicators, new peaks appeared at 12.7°, 25.7°, 39°, and 52.4°. According to the reference (JCPDS #80-1000), the peaks were identified as the peaks of the (001), (011), (110), and (004) planes of PbI_2, respectively. In this stage, decomposition of $CH_3NH_3PbI_3$ into PbI_2 was in progress, showing coexistent peaks from $CH_3NH_3PbI_3$ and PbI_2. For the sample that was stored for 1 month, all of the peaks from the perovskite film appeared extinguished, leaving only the peaks from PbI_2 and FTO. Especially, the intensity of the (001) plane of PbI_2 at 12.7° was significantly higher than the other peaks, although it is not fully depicted in the graph, indicating the well-crystallized formation of PbI_2 because of the complete decomposition of the perovskite film. However, practically no change in the XRD patterns was observed for the hydrophobically passivated perovskite film, as shown in Figure 3b. The passivated film exhibited identical XRD patterns to the untreated film, despite the presence of the passivation layer. These characteristic peaks of the perovskite layer were also found intact in the films after 15 and 30 days. This XRD result analytically supported that the degradation of the perovskite film was effectively prevented by the hydrophobic passivation layer.

Degradation of perovskite into PbI_2 would result in a decrease in the mass of the film caused by the removal of CH_3NH_2 and I_2 molecules, which is obvious when considering the mass differences of perovskite ($CH_3NH_3PbI_3$ = 619.98 g mol^{-1}) and PbI_2 (461 g mol^{-1}). Therefore, degradation of the perovskite film can be investigated by measuring the change in the mass of the film. Because the mass of the perovskite thin film (<~300 nm) is considerably small and difficult to measure, a quartz crystal microbalance (QCM) was introduced to measure the mass change of the film. In a QCM measurement, an increase or decrease in the mass of the sample on a quartz resonator can be detected by the change in the frequency of the resonator. Thus, the increase in the mass of the sample results in the decrease in the frequency, and vice versa. As represented in the scheme in Figure 3c, the TiO_2 mesoporous layer, perovskite film, and Spiro-OMeTAD layer were deposited on a quartz resonator as they were used in the PSC. Two samples were prepared, and the additional hydrophobic passivation was conducted on one of the samples. Without the Teflon-passivation, it was predicted that the moisture in the air would penetrate into the perovskite layer, causing dissolution and evaporation of the methylamine and iodine molecules. The Teflon-passivated film was expected to exhibit insignificant changes in frequency.

The changes in the frequencies were measured under atmospheric conditions, and the obtained curves are shown in Figure 3d. Without the passivation, the film exhibited a continuous increase in the frequency (thus, a decrease in the mass of the film) and, finally, approached a plateau slope (at this point, the color of the film was pure yellow). The passivated film exhibited a relatively irregular curve with many increasing and decreasing regions, but the absolute value of the frequency change did not exceed 500 Hz, whereas the untreated film showed a steady increase in the frequency over 2000 Hz. The irregular curve of the Teflon-passivated film is considered to be derived from the unstable indoor humidity and the experimental noise. However, note that the curve varies in a highly restricted scope (<500 Hz), indicating the negligible change in the mass of the film.

It was possible to perform quantitative analysis of the mass change through a well-known principle explaining the relationship between the mass change and the frequency change, which is the Sauerbrey equation. The equation is $\Delta f = -(2f_0^2/A(\rho_q\mu_q)^{1/2})\Delta m$ where f_0 is the resonant frequency, A is the

DOI: 10.1021/acsami.5b04490
ACS Appl. Mater. Interfaces 2015, 7, 17330−17336

piezoelectrically active crystal area, ρ_q is the density of quartz, and μ_q is the Shear modulus of an AT-cut quartz crystal. However, the equation should be used carefully with the assurance of satisfaction for the following three requirements: rigidity of the deposited mass, uniformity of mass distribution, and minimization of the proportion of the frequency change ($\Delta f/f < 0.02$). In this study, only a qualitative comparison was performed rather than a quantitative comparison because of the followings: (i) the slight suspicion of nonuniformity of mass distribution of the films on the resonator, and (ii) it was considered meaningless to calculate the mass changes because the initial masses of the pristine perovskite film and the passivated film might be slightly different.

Thus far, we discussed the strongly enhanced stability of the perovskite film by hydrophobic passivation. However, if the PCE of a cell is damaged during the passivation process, then the treatment would not necessarily be considered successful. To clarify this issue, $J-V$ curves of the cells before and after the passivation were measured and plotted in Figure 4a. Fortunately, negligible changes in the parameters of J_{sc}, V_{oc}, FF, and efficiency were found in the passivation process. Before the passivation, the cell had a J_{sc} of 18.4 mA/cm^2, V_{oc} of 0.90 V, FF of 0.68, and PCE of 11.3%. After the passivation, the cell had a J_{sc} of 17.9 mA/cm^2, V_{oc} of 0.91 V, FF of 0.72, and PCE of 11.8%. Teflon coating on the top of the cell appeared to have no detrimental effects on photovoltaic performances, except for the reinforcement of stability.

Encouraged by the positive result, time-dependent changes of the PCE were also recorded in a certain interval. The untreated and passivated cells were fabricated and stored under normal indoor conditions. Then, $J-V$ curves of the cells were measured every day followed by plotting of the estimated PCEs, depending on the time in Figure 4b. For clarity, the PCEs of both of the cells were normalized (the initial PCE of the untreated cell was 11.3% and that of the passivated cell was 11.8%). As previously observed, severe degradation of the untreated perovskite cell by humidity was observed, resulting in the steeply decreasing PCE in which 30% of the initial PCE was diminished after only 15 days, and nearly 50% was diminished after 30 days. On the contrary, the PCE of the passivated cell exhibited nearly constant values over the 30 days. The PCE at 30 days was 95% of the initial PCE, suggesting a surprisingly enhanced stability in an ambient atmosphere.

In Figure 4c,d, and Table 1, more detailed information on the degradation of the photovoltaic performance of both of the cells is given. Figure 4c shows the $J-V$ curves of the untreated perovskite cell, measured immediately after cell fabrication, after 7, 15, and 30 days of storage in an ambient atmosphere. Considering the dramatic decrease in the PCE, the V_{oc} of the cell showed a relatively minor decrease. The V_{oc} of the cell was obtained as 0.90 V at the initial stage, 0.89 V 7 days after storage, 0.872 V 15 days after storage, and 0.866 V 30 days after storage. During the degradation, $CH_3NH_3PbI_3$ and PbI_2 coexisted in the absorber layer, appearing to cause negative behaviors of the cell, such as recombination of electron−hole pairs and accumulation of space charges, by increased defects. This results in the J_{sc} degradation of the cell to be relatively serious (initially 18.4 mA/cm^2 then 16.9, 14.0, and 13.0 mA/cm^2, immediately after cell fabrication, after 7 days of storage in an ambient atmosphere, after 15 days, and after 30 days of storage, respectively). Because of the many defects, a severe decline of the fill factor was also observed (0.68, 0.68, 0.64, and 0.56). More profound analyses on the degradation of the cell and the corresponding changes in the photovoltaic parameters will be further researched.

Table 1. Photovoltaic Parameters Concerned with PCE Performances of the PSC and Teflon-PSC, Varying with the Storage Time

cell ID-day	V_{oc} (V)	J_{sc} (mA cm^{-2})	FF (%)	eff (%)
PSC-0	0.90	18.4	68	11.3
PSC-7	0.89	16.9	68	10.2
PSC-15	0.87	14.0	64	7.8
PSC-30	0.87	13.0	56	6.3
Teflon-PSC-0	0.92	17.9	72	11.8
Teflon-PSC-7	0.91	18.1	70	11.5
Teflon-PSC-30	0.87	17.8	72	11.1

Figure 4d shows $J-V$ curves of the hydrophobic passivated cell, which exhibited a relatively negligible degree of degradation during the long-term storage. Even 30 days after the cell fabrication, all of the photovoltaic parameters remained at acceptable degrees. The V_{oc} values of the cell were obtained as 0.92, 0.91, and 0.87 V, sequentially, whereas the J_{sc} values were estimated at 17.9, 18.1, and 17.8 mA/cm^2. The fill factor was also relatively stable at 0.72, 0.70, and 0.72. Without the effective prevention of infiltration of H_2O into the absorber layer, it is impossible to explain this enhanced stability of the cell performance. From the measured $J-V$ curves, it could be concluded that blocking the entry of H_2O into the cell by the hydrophobic passivation was successful. Table 1 summarizes the photovoltaic parameters concerned with PCE performances of the PSC and Teflon-PSC, varying with the storage times. Additionally, $J-V$ curves and stabilized efficiencies of the PSC and Teflon-PSC stored in humidity-controlled atmosphere (at humidity of 50%) were measured and provided in the Supporting Information, Figure S3. In the humid environment, both cells exhibited similar tendency with the results of previous atmospheric environmental experiments.

CONCLUSIONS

In this study, an effective passivation for PSCs using the hydrophobic polymer Teflon was reported. Teflon was deposited onto the top side of the conventional PSC by the simple spin-coating and drying process. This polymer layer repelled H_2O molecules in an ambient atmosphere, resulting in a significantly enhanced stability of the PSCs. The prevention of degradation of the perovskite film was demonstrated by the XRD measurement and QCM analysis. The perovskite film without Teflon exhibited decomposition into the PbI_2 film, as revealed by the characteristic peaks of the XRD pattern. Additionally, a decreased mass in the film obtained from the QCM measurement supported the observation. A negligible change occurred in the Teflon-treated perovskite film, as shown in the unchanged XRD patterns and the constant film mass. Therefore, the PCE of the untreated PSC decreased continuously from 11.3% in the initial test to 6.3% after 30 days, whereas the PCE of the Teflon-PSC exhibited considerably stable performances retaining 95% of the initial PCE after 30 days. It is expectable a positive synergy effect of this passivation method and conventional encapsulation strategies when they are used together. On the basis of this study, we hope it is possible to develop more stable PSCs with the possibility of commercialization after additional complementary studies.

DOI: 10.1021/acsami.5b04490
ACS Appl. Mater. Interfaces 2015, 7, 17330−17336

■ ASSOCIATED CONTENT

Supporting Information

More data including $J-V$ curves of Teflon-PSC after washing, hysteresis investigation of initial PSC, and stabilized efficiency graphs of pristine PSC and Teflon-PSC under humidity-controlled storage. The Supporting Information is available free of charge on the ACS Publications website at DOI: 10.1021/acsami.5b04490.

■ AUTHOR INFORMATION

Corresponding Author

*K. Yong. E-mail: kyong@postech.ac.kr. Tel.: +82-54-279-2278. Fax: +82-54-279-8619.

Notes

The authors declare no competing financial interest.

■ ACKNOWLEDGMENTS

This work was supported by the National Research Foundation of Korea (2013-R1A2A2A05-005344).

■ REFERENCES

(1) Im, J.-H.; Lee, C.-R.; Lee, J.-W.; Park, S.-W.; Park, N.-G. 6.5% Efficient Perovskite Quantum-Dot-Sensitized Solar Cell. *Nanoscale* **2011**, *3*, 4088−4093.

(2) Mitzi, D. B. Synthesis, Structure, and Properties of Organic-Inorganic Perovskites and Related Materials. *Prog. Inorg. Chem.* **2007**, *48*, 1−121.

(3) Baikie, T.; Fang, Y.; Kadro, J. M.; Schreyer, M.; Wei, F.; Mhaisalkar, S. G.; Graetzel, M.; White, T. J. Synthesis and Crystal Chemistry of the Hybrid Perovskite (Ch3nh3)Pbi3 for Solid-State Sensitised Solar Cell Applications. *J. Mater. Chem. A* **2013**, *1*, 5628−5641.

(4) Burschka, J.; Pellet, N.; Moon, S.-J.; Humphry-Baker, R.; Gao, P.; Nazeeruddin, M. K.; Grätzel, M. Sequential Deposition as a Route to High-Performance Perovskite-Sensitized Solar Cells. *Nature* **2013**, *499*, 316−319.

(5) Jeon, N. J.; Noh, J. H.; Kim, Y. C.; Yang, W. S.; Ryu, S.; Seok, S. I. Solvent Engineering for High-Performance Inorganic−Organic Hybrid Perovskite Solar Cells. *Nat. Mater.* **2014**, *13*, 897−903.

(6) Etgar, L.; Gao, P.; Xue, Z.; Peng, Q.; Chandiran, A. K.; Liu, B.; Nazeeruddin, M. K.; Grätzel, M. Mesoscopic Ch3nh3pbi3/Tio2 Heterojunction Solar Cells. *J. Am. Chem. Soc.* **2012**, *134*, 17396−17399.

(7) Mahmood, K.; Swain, B. S.; Jung, H. S. Controlling the Surface Nanostructure of Zno and Al-Doped Zno Thin Films Using Electrostatic Spraying for Their Application in 12% Efficient Perovskite Solar Cells. *Nanoscale* **2014**, *6*, 9127−9138.

(8) Bi, D.; Boschloo, G.; Schwarzmuller, S.; Yang, L.; Johansson, E. M. J.; Hagfeldt, A. Efficient and Stable Ch3nh3pbi3-Sensitized Zno Nanorod Array Solid-State Solar Cells. *Nanoscale* **2013**, *5*, 11686−11691.

(9) Mahmood, K.; S. Swain, B.; Amassian, A. Double-Layered Zno Nanostructures for Efficient Perovskite Solar Cells. *Nanoscale* **2014**, *6*, 14674−14678.

(10) Kojima, A.; Teshima, K.; Shirai, Y.; Miyasaka, T. Organometal Halide Perovskites as Visible-Light Sensitizers for Photovoltaic Cells. *J. Am. Chem. Soc.* **2009**, *131*, 6050−6051.

(11) Kim, H.-S.; Lee, C.-R.; Im, J.-H.; Lee, K.-B.; Moehl, T.; Marchioro, A.; Moon, S.-J.; Humphry-Baker, R.; Yum, J.-H.; Moser, J. E. Lead Iodide Perovskite Sensitized All-Solid-State Submicron Thin Film Mesoscopic Solar Cell with Efficiency Exceeding 9%. *Sci. Rep.* **2012**, *2*, 591.

(12) NREL. NREL Efficiency Chart. http://www.nrel.gov/ncpv/images/efficiency_chart.jpg.

(13) Ito, S.; Tanaka, S.; Manabe, K.; Nishino, H. Effects of Surface Blocking Layer of Sb2s3 on Nanocrystalline Tio2 for Ch3nh3pbi3 Perovskite Solar Cells. *J. Phys. Chem. C* **2014**, *118*, 16995−17000.

(14) Grätzel, M. The Light and Shade of Perovskite Solar Cells. *Nat. Mater.* **2014**, *13*, 838−842.

(15) Fakharuddin, A.; Di Giacomo, F.; Ahmed, I.; Wali, Q.; Brown, T. M.; Jose, R. Role of Morphology and Crystallinity of Nanorod and Planar Electron Transport Layers on the Performance and Long Term Durability of Perovskite Solar Cells. *J. Power Sources* **2015**, *283*, 61−67.

(16) Noh, J. H.; Im, S. H.; Heo, J. H.; Mandal, T. N.; Seok, S. I. Chemical Management for Colorful, Efficient, and Stable Inorganic−Organic Hybrid Nanostructured Solar Cells. *Nano Lett.* **2013**, *13*, 1764−1769.

(17) Smith, I. C.; Hoke, E. T.; Solis-Ibarra, D.; McGehee, M. D.; Karunadasa, H. I. A Layered Hybrid Perovskite Solar-Cell Absorber with Enhanced Moisture Stability. *Angew. Chem., Int. Ed.* **2014**, *53*, 11232−11235.

(18) Habisreutinger, S. N.; Leijtens, T.; Eperon, G. E.; Stranks, S. D.; Nicholas, R. J.; Snaith, H. J. Carbon Nanotube/Polymer Composites as a Highly Stable Hole Collection Layer in Perovskite Solar Cells. *Nano Lett.* **2014**, *14*, 5561−5568.

(19) Xiao, Y.; Han, G.; Chang, Y.; Zhou, H.; Li, M.; Li, Y. An All-Solid-State Perovskite-Sensitized Solar Cell Based on the Dual Function Polyaniline as the Sensitizer and P-Type Hole-Transporting Material. *J. Power Sources* **2014**, *267*, 1−8.

(20) Leijtens, T.; Eperon, G. E.; Pathak, S.; Abate, A.; Lee, M. M.; Snaith, H. J. Overcoming Ultraviolet Light Instability of Sensitized Tio2 with Meso-Superstructured Organometal Tri-Halide Perovskite Solar Cells. *Nat. Commun.* **2013**, *4*, 4885.

(21) Chander, N.; Khan, A.; Chandrasekhar, P.; Thouti, E.; Swami, S. K.; Dutta, V.; Komarala, V. K. Reduced Ultraviolet Light Induced Degradation and Enhanced Light Harvesting Using Yvo4: Eu3+ Down-Shifting Nano-Phosphor Layer in Organometal Halide Perovskite Solar Cells. *Appl. Phys. Lett.* **2014**, *105*, 033904.

(22) Ha, T.-J.; Kiriya, D.; Chen, K.; Javey, A. Highly Stable Hysteresis-Free Carbon Nanotube Thin-Film Transistors by Fluorocarbon Polymer Encapsulation. *ACS Appl. Mater. Interfaces* **2014**, *6*, 8441−8446.

(23) Liu, D.; Kelly, T. L. Perovskite Solar Cells with a Planar Heterojunction Structure Prepared Using Room-Temperature Solution Processing Techniques. *Nat. Photonics* **2014**, *8*, 133−138.

(24) Snaith, H. J.; Abate, A.; Ball, J. M.; Eperon, G. E.; Leijtens, T.; Noel, N. K.; Stranks, S. D.; Wang, J. T.-W.; Wojciechowski, K.; Zhang, W. Anomalous Hysteresis in Perovskite Solar Cells. *J. Phys. Chem. Lett.* **2014**, *5*, 1511−1515.

(25) Niu, G.; Guo, X.; Wang, L. Review of Recent Progress in Chemical Stability of Perovskite Solar Cells. *J. Mater. Chem. A* **2015**, *3*, 8970−8980.

(26) Frost, J. M.; Butler, K. T.; Brivio, F.; Hendon, C. H.; van Schilfgaarde, M.; Walsh, A. Atomistic Origins of High-Performance in Hybrid Halide Perovskite Solar Cells. *Nano Lett.* **2014**, *14*, 2584−2590.

(27) Ren, Z.; Ng, A.; Shen, Q.; Gokkaya, H. C.; Wang, J.; Yang, L.; Yiu, W.-K.; Bai, G.; Djurišić, A. B.; Leung, W. W.-f. Thermal Assisted Oxygen Annealing for High Efficiency Planar Ch3nh3pbi3 Perovskite Solar Cells. *Sci. Rep.* **2014**, *4*, 6752.

(28) Niu, G.; Li, W.; Meng, F.; Wang, L.; Dong, H.; Qiu, Y. Study on the Stability of Ch3nh3pbi3 Films and the Effect of Post-Modification by Aluminum Oxide in All-Solid-State Hybrid Solar Cells. *J. Mater. Chem. A* **2014**, *2*, 705−710.

DOI: 10.1021/acsami.5b04490
ACS Appl. Mater. Interfaces 2015, 7, 17330−17336